Taylor & Francis
Taylor & Francis Group

Temporal analysis of forest structural condition at an acid mine site using multispectral digital camera imagery

P. COSMOPOULOS

Epsilon International SA, 27 Monemvasias, Marousi, Athens, Greece 15125;
e-mail: ycosmos@otenet.gr

and D. J. KING*

Department of Geography and Environmental Studies, Carleton University,
1125 Colonel By Drive, Ottawa, Ontario Canada K1S 5B6;
e-mail: doug_king@carleton.ca

Abstract. A large abandoned tailings deposit at a mine site near Timmins, Ontario, Canada has produced significant damage in an adjacent forest due to contamination and wind stress. Significant forest structure changes were measured between 1997 and 1999. A multivariate image-based forest structure index (FSI) was developed using canonical correlation analysis of 1997 field and airborne digital camera data. FSI included decreasing canopy closure and leaf area index, and increasing blown down and standing dead structure measures associated with image spectral, textural and radiometric fraction variables. An image model predicting FSI achieved an $R^2 = 0.66$. The model equation was then applied to 1999 airborne imagery to predict FSI for each plot. Comparing the 1999 image predicted FSI to that calculated from field data showed that the model was strong in predicting positive or no forest structure changes, but not increased structure degradation. The latter was due to the presence of herbaceous and shrub vegetation that had developed during the two-year period in open plots near the tailings where blow down was significant. The next research phase will derive means to separate these two signals in forests of open overstory.

1. Introduction

Much effort has been made to develop methods for measurement of individual forest structure parameters using remote sensing. In forest management, tree size (height and diameter) and stem density are of primary importance for growth and wood volume information needs. In ecology and climate modelling, leaf area index (LAI), per cent cover and other measures of biomass quantity are used. Each of these individual variables is often fed into a production model to determine some output variable such as the potential wood product value or carbon budget status. However, forest structure is an integrated composite of individual tree structure,

---

*Corresponding author.

quantity, and arrangement in the landscape in both horizontal and vertical dimensions. This research attempts to develop an integrated measure of forest structure as an index comprising several variables that can be measured and monitored using remote sensing.

While many forest management information needs for inventory are met using aerial photography (Gillis and Leckie 1993, King 2000), modelling of individual forest structure variables such as LAI, canopy closure, crown diameter, basal area, and stem density has been conducted using both airborne and satellite imagery. The most common approach has been to use spectral information such as vegetation indices (Gong *et al*. 1995, Lawrence and Ripple 1998, Haddow *et al*. 2000, Chen *et al*. 2002). Addition of image spatial information, particularly using airborne data, has generally improved these models significantly. Image texture (Yuan *et al*. 1991, Wulder *et al*. 1997, Olthof and King 1997), spatial dependence (e.g. semivariance range) (Cohen and Spies 1990, St. Onge and Cavayas 1995, 1997, Wulder *et al*. 1998, Lévesque and King 1999) and radiometric fractions derived at the pixel level using clustering (Pellikka *et al*. 2000, Seed and King 2003) or at the subpixel level using spectral unmixing (Hall *et al*. 1996, Peddle *et al*. 1999, Lévesque and King 2003) are the most commonly studied image spatial information types for this purpose.

Representation of forest structure as a multivariate composite of various parameters has been presented by Everham (1996) and Ferretti (1997). Both of these studies assessed forest structure in the context of structural health, the former in relation to wind damage, and the latter as an indicator of forest vigour. Franklin (2000) summarizes other studies that have taken this approach. Extending this concept of a composite structure index to measurement using remote sensing has been attempted, but generally with spectral information only. For example, Franklin (2000) summarizes studies relating vegetation indices and the TM wetness index to a few structural indices. Jakubauskas (1996) found that more than half the variance of a coniferous forest canonical variate representing LAI, basal area and stem density could be explained by Landsat Thematic Mapper (TM) spectral information. Integration of image spatial information into such modelling has been less frequent. An example is Yuan *et al*. (1991) who defined a tree decline index based on visual photographic interpretation of spectral damage symptoms (e.g. chlorosis, visible dead branches) and crown texture (rougher textures representing more open crowns) and then modelled this index using airborne video spectral and textural information. Another was presented by Cohen and Spies (1992) to represent a structural complexity index using semivariance analysis. In this paper, aspects of these approaches are combined in multivariate modelling to develop a forest structural condition index using high-resolution airborne imagery. Canonical correlation analysis is used to relate forest structure variations caused by blow down and contamination at an abandoned mine to image spectral, textural, and radiometric fraction information. The image model is applied to data acquired in 1997 and 1999 and its effectiveness in prediction of temporal change in forest structure is evaluated.

2. Objectives

The study is part of a long-term research project initiated in 1992 (King 2002) to develop remote sensing methods for assessment and monitoring of forest damage at an abandoned mine site near Timmins, Ontario. The goal of this study was to examine the feasibility of employing a multivariate image-based forest structural

condition index for monitoring the effects of a large sulphide tailings deposit on forest health. The objectives of the research are as follows.

1. Assess whether significant forest structural change had taken place at the study site between 1997 and 1999. Previous observations at the site had shown it to be very dynamic so significant changes in forest structure and tree mortality were expected during this two-year period.
2. Given forest change is significant, develop a multivariate model relating various forest parameters indicative of the structural health at the site and airborne digital camera spectral and spatial information.
3. Apply the model to 1997 and 1999 imagery to predict forest structure changes throughout the study site and evaluate the prediction accuracy.

3. Study area

The study area is located near the abandoned copper-zinc deposit of the Kam-Kotia Mine north-west of Timmins, in northern Ontario (figure 1). Surrounding the mine are three tailings areas covering about 350 ha. The study area is a forest approximately 1.4 km (east–west) by 800 m (north–south) adjacent to the north unimpounded tailings as shown in figure 1. It is bounded by the Northwest creek, East creek, and tailings edge, each being visible in figures 1, 2 and 4. Topographically, most of the area surrounding the mine is relatively flat and is characterized by poor drainage, forming swamps and meandering streams. Drainage follows a slight elevation gradient from the north impounded tailings through the north unimpounded tailings and towards the study area in the north-east. Outflow drainage from the tailings is collected in the Northwest and East creeks, which join to flow into the Kamiskotia River.

The study area is a typical mixed boreal forest. An overstory canopy of mature
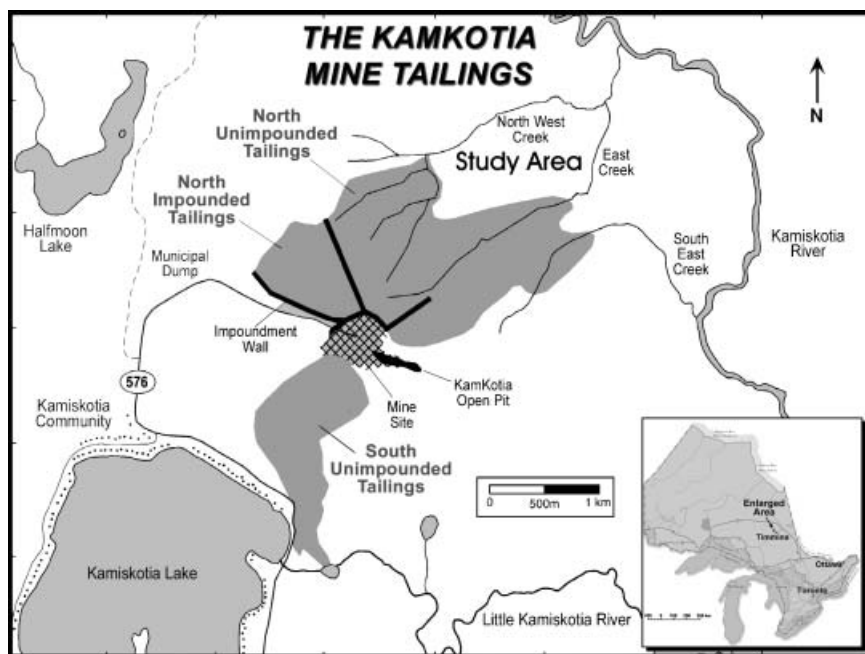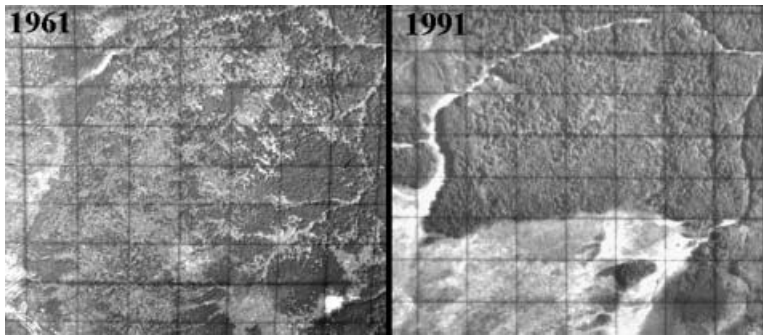

Figure 1.   Study area.

Figure 2. Study area before tailings deposition (1961) and 17 years after mine abandonment (1991) (Ontario Ministry of Natural Resources air photographs).

trembling aspen (*Populus tremuloides*) dominates most of the drier areas, while white birch (*Betula papyrifera*) and black spruce (*Picea mariana*) cover the wetter areas. An understory of balsam fir (*Abies balsamifera*) is also present in some of the more mature areas. Figure 2 shows two aerial photographs of the study area, the first in 1961 prior to the tailings deposition, and the second in 1991.

Visible signs of forest damage are mostly structural and include: (1) uprooted and snapped trees, resulting from strong winds that develop over the open tailings, (2) dead branches and standing dead trees, (3) undersized crowns, and (4) high crown and canopy openness. Thin, open crowns are particularly obvious near the tailings, possibly due to contaminants deposited by wind and/or drainage. Figure 3 illustrates forest contamination by drainage and wind, as well as mechanical wind stress effects. Lévesque and King (1999) found decreasing gradients of several soil metals with distance from the tailings.

In previous studies at the site relevant to this paper, Walsworth and King (1999) analysed aerial photography from 1961 to 1991 using a spatially explicit individual
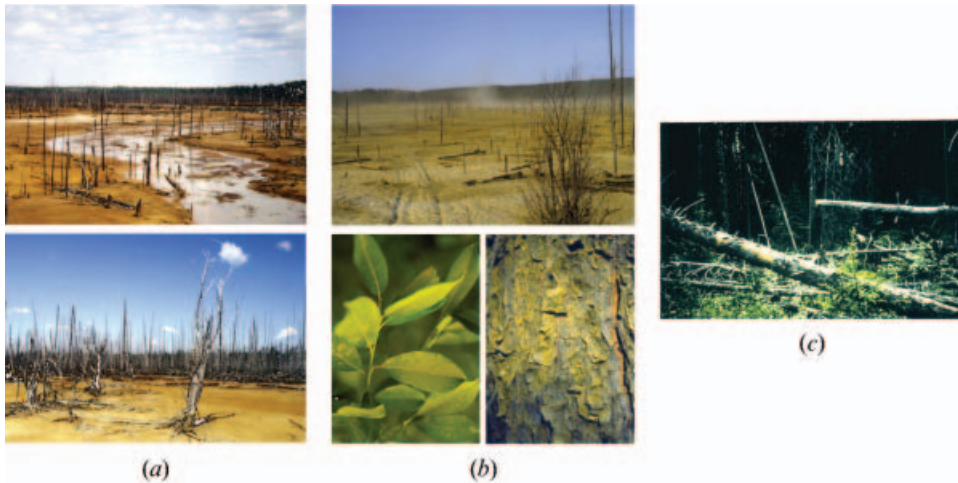

Figure 3. Forest stress types at the study site. (*a*) Acid mine drainage into the adjacent forest in runoff and groundwater, (*b*) tailings dust and deposition on bark and leaves in the forest, (*c*) blown down trees in the study area about 50 m from the tailings' edge.

tree based transition model. They found that the area within about 200 m of the tailings edge exhibited a trend towards continued growth of pioneer, light intolerant species such as aspen, while further from the tailings, succession was towards a more closed canopy which conifers were beginning to infill. Seed and King (1997) found strong relations between 25 cm pixel digital camera radiometric fractions (deep shadow, transitional shadow on crown edges and within crown shadow) and effective LAI (LAI assuming a random leaf orientation and referred to herein simply as LAI). Subsequently, they found that shadow brightness was more related to LAI than the commonly used shadow fraction because it is more robust over varying view angles and is sensitive to varying amounts of understory (Seed and King 2003). Olthof and King (1997), using the same data, found complementarity between texture and texture spatial variation in modelling of LAI. Olthof and King (2000) then incorporated the findings from these studies in the development of a forest health index (herein called a forest structure index, FSI) using multivariate analysis of groups of these image variables against groups of forest variables representing the structural damage evident at the site. This study extends the research of Olthof and King by refining the FSI formulation and applying it in a temporal analysis of forest change at the site.

4. Methods

4.1. *Field data and analysis of forest change*

In the summers of 1997 and 1999, field measurements were taken in 44 plots of 10 m radius ($314 m^2$) each, located along six parallel transects labelled A to F from east to west (figure 4). The beginning of each transect is located at the edge of the tailings and the transect lengths range from 350 m to 850 m. The plots were located at 10 m, 60 m, 110 m, 210 m, 310 m, 410 m, 510 m and 710 m from the tailings' edge. The sampling scheme was spatially biased, including more plots in the area near the tailings' edge, because previous research in the study area (Lévesque and King 1999, Walsworth and King 1999, Olthof and King 2000) had found greater forest damage closer to the tailings' edge.

In each plot, all trees taller than 2 m were counted, species were identified, and diameter at breast height (DBH) was measured. The status of the standing trees was
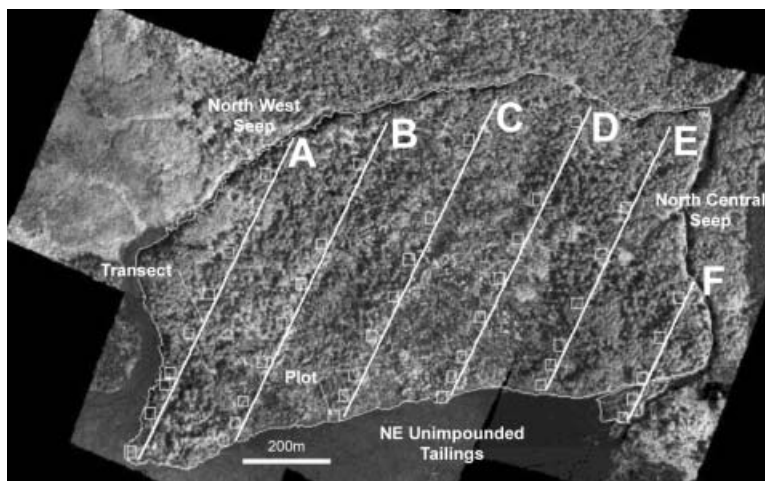

Figure 4. Mosaic of 1999 NIR band images of the study area with study plots delineated.

assessed visually to distinguish between live (presence of foliage) and dead trees. After all standing trees in a plot were assessed, the same data were acquired for all fallen trees. The stem density and basal area of standing live, standing dead and fallen trees were calculated for each plot.

A Li-Cor LAI-2000 Plant Canopy Analyser was used to measure forest canopy closure and (effective) LAI. A sensor was placed in the open as a reference of open sky and another was used in the forest. Measurements were taken at dusk and dawn under diffuse sky conditions. The LAI-2000 estimates the total gap fraction at different angles (Li-Cor, Inc. 1991) using hemispherical optics and a ringed detector that simultaneously measures diffuse radiation in five distinct angular bands, centred at $7°$, $22°$, $38°$, $52°$, and $68°$ about the zenith. The narrowest view angle $0°–15°$ represents a number of sample points penetrating the canopy directly above and therefore is used to estimate canopy closure. The first three rings give the best estimate for LAI (Li-Cor, Inc. 1991) but the first four rings may also be useful. The measurements were taken in mid to late August 1997 and 1999 to coincide with the time of image acquisition. The 1997 field data had been previously acquired for the study by Olthof and King (2000). The study plots represented diverse forest conditions of varied composition. For example, in 1997, canopy closure ranged from 12% to 90%, and LAI from 0.41 to 5.03. The ranges of numbers of blown down, standing dead and standing live stems per plot were 0–36, 0–39, and 5–118, respectively. The complete set of forest structure variables used in the study is listed in table 1.

An analysis of the field data was conducted to determine if real forest structural changes had occurred in the 1997–1999 period. This would justify the image-based temporal analysis for such a short time period. Each forest variable was assessed using Student t-tests to determine if the differences between the means of 1997 and 1999 were significant. Processing for outliers and to transform variables to Gaussian distributions was conducted. A comparison of these data for the area within 210 m of the tailings and the area beyond 210 m was also conducted. Walsworth and King (1999) had found this to be the approximate distance in which impacts of the tailings were severe.

Table 1. Forest structure and image variables for 36 field plots and image subscenes.

| Image variables		Forest structure variables	
Spectral		*Stem density (stems/plot)*	
B_{NIR}	Average NIR brightness	Lstem	Live stem density
B_R	Average red brightness	Dstem	Dead stem density
B_G	Average green brightness	Bdstem	Blow down stem density
B_B	Average blue brightness		
NDVI	$(B_{NIR}-B_R)/(B_{NIR}+B_R)$		
Radiometric fractions		*Basal area (m^2/plot)*	
S1	Deep shadow	Lbasal	Live basal area
S2	Transitional shadow	Dbasal	Dead basal area
S3	Sunlit crown	Bdbasal	Blow down basal area
Contrast texture		*Li-Cor measurements*	
Tex_R	Average red band texture	LAI3	LAI (rings 1–3)
Tex_G	Average green band texture	LAI4	LAI (rings1–4)
$Texs_R$	Red band texture standard deviation	Closure	Canopy closure (ring 1)
$Texs_G$	Green band texture standard deviation		
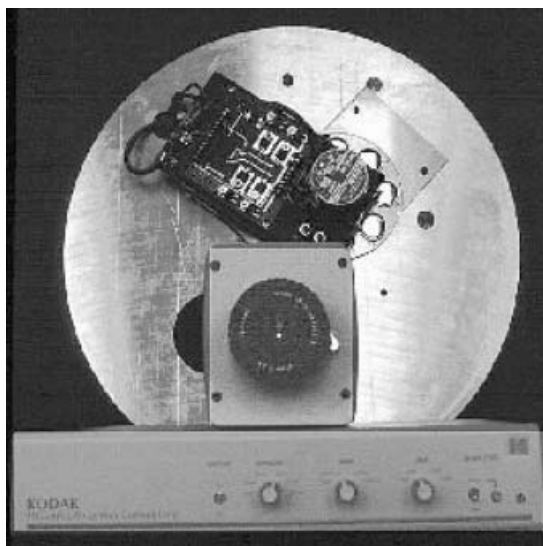
Figure 5. Multispectral digital camera sensor (King 1995).

4.2. *Image acquisition and data processing*

A multispectral digital sensor (AMDFCS, figure 5) incorporating a Kodak Megaplus 1.4 black-and-white, 1300×1000 pixel format camera was used for image acquisition (King 1995). A rotating filter wheel in front of a 28 mm focal length lens provided a total view angle of $18.2° \times 14.3°$ and 8-bit data in up to eight spectral bands of $\geqslant 10$ nm bandwidth within the range of 450 nm to 900 nm. Imagery of the study area was acquired with 25 cm, 50 cm and 80 cm pixel sizes on 18 August 1997 (Olthof and King 2000) and 19 August 1999.

The pixel size of the imagery in this study was 50 cm. Four spectral bands were used as follows: blue (B: 430–470 nm), green (G: 545–555 nm), red (R: 665–675 nm), and near-infrared (NIR: 895–905 nm). Images were acquired on four flight lines covering the area with adequate forward and side overlap. Band offsets due to filter wheel rotation were corrected by aligning three of the bands in each multispectral set to the fourth (reference band) using a minimum of four ground control points (GCPs) and a first-order transformation.

Brightness variations due to sun angle and optical effects were corrected in each image using an algorithm that determined the mean of each image column, fitted a polynomial (second order was selected) to the set of means crossing the image and inverted the polynomial to normalize the brightness values across the image (PCI Inc. 1994). This correction was applied in both image directions. Figure 6 shows an example of a 1999 image before and after correction.

Mosaics were then assembled from the 1997 and 1999 data. Ten scenes were sequentially combined in each mosaic using a minimum of four ground control points (GCPs) for each pair of images and a first order transformation. Average RMS error in mosaic processing was approximately one-half the pixel dimension (25 cm). Histograms of each image pair were also matched in the overlap area to remove brightness differences at seams. Figure 4 shows the NIR band of the 1999 mosaic with plots delineated.

The 1999 mosaic was georeferenced to a UTM projection using eight GCPs that
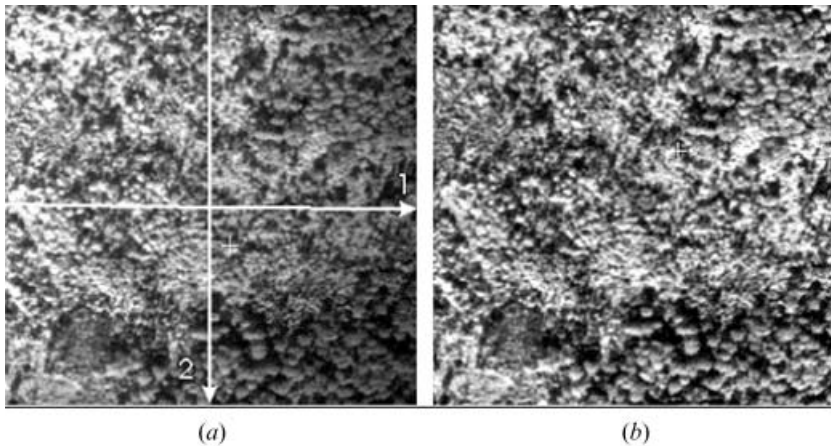
Figure 6. Example of radiometric corrections on a 1999 image frame: (*a*) uncorrected image and (*b*) corrected image.

consisted of 2 m white square targets placed in the field before the flight and surveyed using real-time differential GPS (*x, y* accuracy ∼0.5 m). A second-order transformation was required in this process, producing an RMS error of 0.10 m. Next, the 1997 mosaic was aligned to the georeferenced 1999 mosaic in an image-to-image registration using 16 control points and a second-order transformation, resulting in an RMS error of 0.15 m. Visual inspection of band histograms revealed that the exposure (overall brightness) of the 1997 imagery was lower than the 1999 imagery, and its brightness range was smaller. The histograms of the two mosaics were therefore matched to provide equivalent mean brightness and standard deviation. This process assumes that there were no gross changes in cover type in the two-year period.

Image subscenes corresponding to the surveyed locations of the field plots were extracted from the georeferenced mosaics. As the pixel size was 50 cm, the subscenes were 40 by 40 pixels. Thirty-six of the forty-four plots were extracted from the imagery where data were available for both 1997 (some plots were missed in 1997 due to aircraft navigation error) and 1999. Once all image subscenes for both dates were radiometrically corrected, image parameters that had previously demonstrated good relationships with forest structure measures at this site (Seed and King 1997, Olthof and King 1997, Olthof and King 2000) were extracted. They included:

1. mean plot brightness in each band (B_{NIR}, B_R, B_G, B_B);
2. three radiometric fractions extracted using an unsupervised classification (ISODATA): deep shadow (S1) between crowns, transitional shadow (S2) on crown edges and within crowns, and sunlit crown (S3);
3. the Normalized Difference Vegetation Index (NDVI);
4. mean and standard deviation of the co-occurrence texture measure 'Contrast' (Haralick 1979) extracted from the red (Tex_R, $Texs_R$) and green (Tex_G, $Texs_G$) bands. This texture measure and texture in these bands provided higher correlations with individual forest structure measures than other measures and bands. A sampling distance of 1 was applied in all directions around the centre pixel (omni-directional) and a 3×3 window was used to maximize information on local texture.
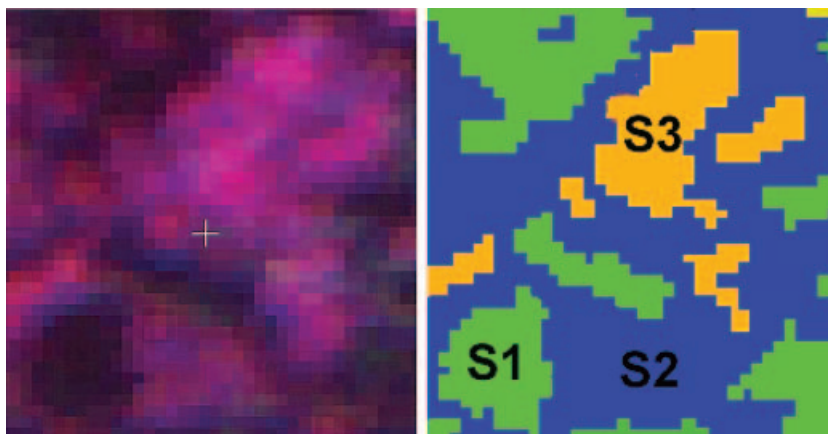
Figure 7.   Colour infrared composite (*a*) and radiometric fractions (*b*) extracted from plot A10, 1997 data. S1 = deep shadow; S2 = transitional shadow; S3 = sunlit crown.

An example of the radiometric fractions extracted for one of the plots is given in figure 7. The 12 image variables are listed with the nine field variables in table 1.

4.3. *Multivariate analysis of forest and image variables*

Canonical correlation analysis (CCA) was used to investigate multivariate linear relationships between forest structure parameters and image parameters in the 1997 data and to form a basis for the development of a forest structure condition index. The method was adapted from Olthof and King (2000) who applied it to the same 1997 data in an initial analysis without the radiometric corrections, differential GPS survey of plot locations and image georeferencing as described above. In this study, these data improvements were expected to strengthen the relations between forest and image variables. Statistical aspects of CCA and principal components analysis (below) are summarized here; additional details are given in Olthof and King (2000). Canonical correlation coefficients that were statistically significant ($\alpha \leqslant 0.05$) were retained for analysis. The canonical correlation between the significant variate pairs is indicative of the strength of the relationship between the variable sets and the squared canonical correlation is the shared variance between a pair of variates. According to Tabachnick and Fidell (1996), canonical correlations lower than 0.30 are generally considered unacceptable as they represent less than 10% shared variance between the variate pairs.

To reduce the ratio of the number of variables to number of plots (samples) and to provide orthogonal variables for CCA, principal component analyses (PCA) of the forest and image data were first conducted. Only the components with eigenvalues greater than 1.0 were retained as suggested for sample sizes less than 50 by Kaiser (1960) and Stevens (1996). These PCs represent variance that is greater than the variance of a single variable (i.e. the PC is useful in representing combined variance of more than one variable). Interpretation of the components was based on the correlations between the variables and the PCs (factor loadings) that were statistically significant. Variables with loadings greater than 0.75 were interpreted, as this threshold is generally equivalent to strong significance ($\alpha = 0.01$) with small

samples ($<$ 50) (Stevens 1996). Varimax rotation (Kaiser 1960), a technique designed to stretch loadings in each PC, was used to improve the interpretability of the PCs.

4.4. *Formulation of an image-based forest structure condition index (FSI)*

In CCA, the canonical variates (CVs) consist of multiple forest variables that are linearly related to multiple image variables. The set of forest structure principal components that formed the most significant canonical variate was selected as an integrated forest structure condition index (FSI) that could be modelled by airborne imagery. Although the relation of FSI to the image canonical variate could be used for predictive purposes, it was desired to develop a predictive model of FSI using an optimal subset of the original image variables (table 1). This was because image principal components are more difficult to interpret, they require extraction of all image parameters, and they do not represent all the variance found in the field data. Consequently, forward stepwise regression was used with the image data (table 1) as independent variables and FSI as the dependent. The goal was to identify a subset of image variables that could best predict the integrated forest structure index. To avoid multicollinearity in the regression process, a variance inflation factor (VIF) of 5.3 was used as a cut-off threshold, which corresponds to correlations (r) exceeding 0.90 between the independent variables (Tabachnick and Fidell 1996, Hair *et al.* 1998).

Normal probability plots of the residuals were also examined for any departures from normality. As a final evaluation, a graph of the standardized residuals versus the predicted values was generated in order to determine the validity of the selected best-fit model, and to check for any departures from linearity or any trends in the residuals.

4.5. *Temporal analysis of 1997–1999 forest change using the field data and the FSI image model*

Once the best-fit regression model was determined for the 1997 plot data, it was applied to both the 1997 and 1999 image data in order to predict FSI for each plot. The difference between the two FSI values for each plot (1999–1997) was used as a measure of image-predicted forest structure change. In the same way, the FSI formulation was applied to both sets of field data. The difference between these two scores (1999–1997) was used as a measure of actual forest change.

Image predicted FSI change was compared to actual FSI change to determine its accuracy and identify issues to be addressed in further refinement of the image-based FSI methodology. For practical purposes (e.g. the Ontario Ministry of Northern Development and Mines wishes to simply know where in the forest degradation is occurring), the comparison was done on a class basis by applying a statistical cluster analysis to both the image predicted and actual forest change datasets. Ward's cluster methodology was used as it most closely mimics biological systems; samples placed into a cluster often represent a common environment (Fishbein and Patterson 1992). It identified distinct forest change clusters and assigned each of the 36 plots to one of the clusters. Clusters were grouped into positive change (improved structure condition), negative change (increased openness and damage) and stable classes. The image-predicted FSI change class for each plot was compared to the actual change class and the frequency of correct and incorrect class assignments was calculated.

5. Results and discussion

5.1. *Analysis of change in forest structure, 1997–1999*

Of the nine forest variables in table 1, eight had significantly changed ($p \leqslant 0.05$) between 1997 and 1999. The numbers of blown down stems increased significantly ($p = 0.01$) as did the basal area of blown down stems ($p = 0.03$). Coinciding with this were significant increases in live stem density ($p = 0.02$), canopy cover ($p < 0.01$) and LAI ($p = 0.03$). However, these stems were mostly small as the live basal area had decreased significantly ($p < 0.01$). Standing dead basal area decreased by an almost significant amount ($p = 0.053$), while the numbers of standing dead stems did not change significantly ($p = 0.94$). This indicates that larger dead trees had fallen while approximately equal numbers of smaller trees had died in the two-year period. These data show that the forest is very dynamic, as significant structural changes have occurred in a short time period. Wind was a primary cause of structural change, blowing down live and dead stems. Many of these stems were large and exposed in the upper canopy leaving reduced live and standing dead basal area. Mortality by contamination or natural causes was not as significant as blow down but was present as a more subtle cause of structural change.

Forest change was also much greater closer to the tailings. For example, within 210 m of the tailings blow down basal area, canopy closure and live stem density increased by 33.7%, 20.2% and 21.8%, respectively. In interior plots further from the tailings' edge, they increased by only 21.8%, 7.3% and 4.5%, respectively. This shows, that blow down was a primary mechanism of structural change throughout the study site and that, near the tailings, significant new growth of small trees had occurred compared to further from the tailings. Much of this new growth consisted of alders and white birch trees that had grown above the measurement threshold of 2 m height and above the LAI-2000 sensor height of 1.5 m. There was also an associated visible increase in ground and shrub vegetation in these open plots that was not measured. These points on temporal-spatial forest structure change are critical to interpretation of the results of remote sensing modelling below.

5.2. *Principal component analyses of forest and image data*

The results of the principal component analyses (PCA) of the 1997 forest structure and image variables are summarized in table 2. The nine forest structure variables were reduced to three components with eigenvalues greater than 1.0, accounting for 81.3% of the total variance. The first component (STR1) represented 41.6% of the variance and was significantly related to LAI and canopy closure.

Table 2. Results of principal component analysis.

Variable set	Component	Significant variables*	Eigenvalue	Cumulative variance (%)
Forest structure	STR1	LAI3, LAI4, Closure, (Lbasal)	3.74	41.55
	STR2	Bdstem, Bdbasal, (Lstem_l)	2.10	64.90
	STR3	Dstem_l, Dbasal_l	1.48	81.38
Image	IM1	$-$NDVI, B_R, (B_B)	4.70	39.15
	IM2	S2, Tex_R, $-$S1, ($Texs_R$)	2.13	56.91
	IM3	Tex_G, $Texs_G$	1.53	69.67
	IM4	B_{NIR}, S3, (B_G)	1.31	80.59

*Variables in parenthesis had high loadings but were less significant (loading < 0.75).

Although the factor loading for live basal area was not significant based on the criterion used ($r > 0.75$), it also increased with increasing LAI and closure ($r = 0.65$). The second structure component (STR2) accounted for 23.3% of the total variance and was related to blow down stem density and blow down basal area. The log of live stem density was somewhat associated with this PC ($r = 0.58$), as in open areas with high blow down, the number of small live trees was generally high. The third component (STR3) explained 16.7% of the data variance and was related to tree die-back and mortality.

The image PCA reduced the set of variables from 12 to 4 components with eigenvalues greater than 1.0. Derived image components represented spectral, textural, and radiometric fraction information, and accounted for 80% of the total data variance. The first component (IM1) accounted for 39.2% of the variance and provided red and NIR spectral information that was inversely related to the amount of vegetation present. Blue band brightness was almost significant and followed the same trend ($r = 0.63$). The second component explained 17.8% of the data variance and was related to red band texture, transitional shadow, and negatively to deep shadow. Red band texture variation was almost significant ($r = 0.59$). The third component explained 12.7% of the data variance and was related to green band texture and texture variation. The fourth component explained 10.9% of the total variance and was related to the sunlit crown fraction, as well as the mean spectral brightness from the near-infrared band (B_{NIR}). Green band brightness was almost significant ($r = 0.65$). This component was directly related to individual tree crown condition.

5.3. *Multivariate analysis of forest and image variables*

In CCA analysis of the 1997 forest and image data, three canonical variate (CV) pairs were extracted, of which the first was statistically significant ($r = 0.73$, $p = 0.01$). This was a significant improvement from the analysis of the raw data in Olthof and King (2000) ($r = 0.35$), demonstrating the importance of the radiometric and geometric corrections applied in this study. The first CV described a linear relation of the three forest structure PCs to the four image PCs as shown in table 3. The image variate (independent) explained 53% ($r^2 = 0.53$) of the variance present in the forest structure variate (dependent). Of the forest structure components, the second (STR2) had the highest loading (0.97), which shows that 94% of its variance was shared with the image variate. The second and third components (STR2 and STR3), representing forest change towards decreased blow down and mortality, respectively, were inversely associated with the first component, which represented live forest volume. This forest structure canonical variate was therefore used as the forest structure condition index (FSI) in subsequent analysis. It is multivariate, measuring several types of forest structure variation, each weighted by the variance accounted for in the relation with the image variate. For the image variate, the second and third components (IM2 and IM3) represent mostly image textural and

Table 3. First canonical variate pair of image and forest structure, 1997 data.

Forest structure canonical variate (FSI)	Image canonical variate	Canonical correlation (r)	Significant (p)
(0.20) STR1, (−0.97) STR2, (−0.12) STR3	(0.18) IM1, (−0.60) IM2, (−0.75) IM3, (0.23) IM4	0.73	0.01

shadow fraction information. They have significantly higher loadings and are inversely related to IM1 and IM4, which represent spectral information and the sunlit crown fraction.

Interpretation of this canonical relation can be made by combining the sign (+ or −) of each variable in its associated principal component (table 2) with the sign of the principal component in the canonical variate (table 3). Using only the significantly loaded ($r > 0.75$) variables for each PC, the interpretation is as follows. Increasing LAI and canopy closure, and decreasing blown down and standing dead stem density and basal area are associated with decreasing image texture, texture variation, transitional shadow fraction, and NDVI, and increasing deep shadow, red and NIR spectral brightness, and the sunlit crown fraction. This interpretation represents decreasing FSI as being associated with increasing openness and damage. All image variables follow expected trends except for the spectral variables of decreasing NDVI and increasing red and NIR brightness, which are difficult to explain. FSI is dominated by blow down as the coefficient of the normalized principal component STR2 is 0.97 versus 0.20 and 0.12 for the other PCs in this variate. In addition, it must be noted, that although live stem density was not as significant as blow down in STR2, it does contribute some variance and increases as FSI decreases. This shows that a trend towards decreased canopy closure (i.e. more canopy openness) is also associated with an increase in small live stems. In this dynamic site, where wind and contaminant stresses are high, observations since 1992 show that these small trees do not generally grow to fill in the upper canopy.

5.4. *Image-based modelling of the FSI*

The results of the multiple regression of FSI against the original image variables (table 1) are summarized in table 4.

One image variable was added in each step of the regression. The combination of the five image variables in the table produced the best-fit model with the highest adjusted R^2 (0.61) and the lowest standard error (0.63). The image variables in the model were: Red band texture and texture variation (Tex_R, $Texs_R$), Green band texture (Tex_G), sunlit crown fraction (S3), and mean brightness from the blue band (B_B). The variance inflation factor (VIF) ranged from 1.22 to 4.74 at each model step, always being less than the cut-off threshold of 5.3. The regression equation was:

$$FSI = -0.18 - 1.21Texs_R + 0.02B_B + 0.45Tex_R + 0.06S3 - 0.35Tex_G \qquad (1)$$

All variables in the equation follow the expected trend with increasing FSI and

Table 4.   Stepwise regression results of FSI (forest structure canonical variate) against image variables, 1997 data.

Step	Variable	R^2	Adjusted R^2	Standard error of estimate	Significance
1	$Texs_R$	0.40	0.38	0.79	0.000
2	B_B	0.48	0.45	0.74	0.028
3	Tex_R	0.56	0.52	0.69	0.023
4	S3	0.61	0.56	0.67	0.059
5	Tex_G	0.66	0.61	0.63	0.034

agree with the canonical analysis except red band texture (Tex$_R$), which increases with increasing FSI. It may be acting as a suppresser variable in the equation, accounting for noise variance in other variables.

5.5. *Temporal analysis of 1997–1999 forest change using the field data and the FSI image model*

FSI calculated from the field data for 1997 and 1999 showed that decreases in FSI representing increased blow down, increased dead stems, and reduced cover and LAI were concentrated near the tailings and in the central bog area along transects B, C and D (figure 4). This area lies at a lower elevation and is characterized by sparse forest cover consisting of black spruce, balsam poplar, and balsam fir. Furthermore, forest degradation has expanded from the tailings towards the north-east, indicating a link with contamination and mechanical stress caused by the tailings' drainage and predominant summer winds (from S to SW).

Image-predicted FSI change and actual FSI change calculated from the field data were subjected to cluster analyses. A dendrogram generated by the cluster analysis showed that for a Euclidean distance of eight, there were three equally spaced equivalent clusters. Each plot in the image-predicted and actual FSI change datasets was assigned to a cluster representing negative change (C1), positive change (C2), or little or no change in FSI (C3). The image model accuracy was 83% in prediction of positive or no change in FSI but only 15% accurate in prediction of negative FSI change. The absolute magnitude of predicted change in FSI was also different to actual FSI change (predicted FSI change tended to be positively biased).

The image model predicted increasing FSI (greater closure and less blow down/mortality) in most plots near the tailings where actual FSI change was negative. This was because of high rates of blow down opening the canopy and providing light for growth of ground vegetation and small trees. Canopy closure within 210 m of the tailings was already quite low in 1997 (41% average compared with 67% further away) meaning that blow down prior to 1997 had reduced the canopy to a level where high amounts of light aided growth of smaller vegetation. The average number of blown down stems per plot measured in 1997 was 11.2 within 210 m of the tailings compared to 7.4 further away. Blow down continued at high rates resulting in 1999 average counts of 18.5 stems per plot within 210 m of the tailings and 10.2 stems per plot further away. With such large openings being constantly created, canopy closure of the overstory was obviously decreasing and growth of ground vegetation and small trees was encouraged, resulting in a large increase in closure to 61% on average within 210 m of the tailings and a smaller increase to 75% further away. This process produced a 'carpet' of vegetation that resulted in image responses of reduced texture and texture variation and increased sunlit fraction, each contributing to a positive change in predicted FSI.

This new vegetation growth encountered in 1999 consisted of pioneer species such as alder, birch, raspberry, other shrubs, and grasses that were comprised of up to hundreds of stems in open plots. Vegetation under 2 m height had not been measured in the field due to time limitations of counting the live stems and difficulty in separately measuring closure and LAI for ground vegetation and overstory measurements using the Li-Cor LAI-2000. In future refinement of the FSI method, it is evident that vegetation smaller than 2 m in height must be measured since it is significantly contributing to the image signal in plots of open overstory.

In addition, at this site, growth of intermediate vegetation into gaps left by fallen dominant trees had not been observed over 7 years. This will be verified quantitatively using methods currently under development for vertical profile structure measurement using hemispheric photographs taken from an extendable pole. Including separate ground, intermediate and overstory structure information in the canonical analysis will probably result in a different formulation of the forest canonical variate (FSI) and relate it to a modified image variate. It will aid in more holistically representing forest changes at all levels in the canopy through image-based modelling.

6. Conclusions

A forest structure condition index (FSI) has been developed that is multivariate, representing leaf area and canopy closure, standing live and dead tree structure, and fallen tree structure. It was developed in relation to high-resolution spectral and spatial image characteristics using canonical correlation analysis. The image parameters were sensitive to 66% of the variance of FSI. This approach to integrated measurement of forest structure using remote sensing is applicable in spatial mapping and temporal monitoring. In the case study of this research, a forest subject to mine contamination and wind stress was analysed over a two-year period during which significant changes in forest structure had been measured. The FSI model developed from imagery of the first date was applied to normalized imagery from the second date to predict FSI change. Successful prediction was achieved for interior forest areas of greater closure that had not changed or that had positively changed towards increasing closure and less mortality/blow down. In open damaged canopies near the tailings, where many overstory trees had fallen or died, the imagery responded to ground vegetation growth that had not been measured in the field due to practical constraints. Thus, where overstory degradation was severe and FSI decreased most, image predicted FSI change was often positive. Future refinement of this multivariate forest condition assessment methodology will include separate measurement of vegetation cover in vertical layers to provide sensitivity to such changes in very open areas.

References

CHEN, J. M., PAVLIC, G., BROWN, L., CIHLAR, J., LEBLANC, S. G., WHITE, P., HALL, R. J., PEDDLE, D., KING, D. J., TROFYMOW, J. A., SWIFT, E., VAN DER SANDEN, J., and PELLIKKA, P., 2002, Validation of Canada-wide LAI maps using ground

measurements and high and moderate resolution satellite imagery. *Remote Sensing of Environment*, **80**, 165–184.

COHEN, W. B., and SPIES, T. A., 1990, Semivariograms of digital imagery for analysis of conifer canopy structure. *Remote Sensing of Environment*, **34**, 167–178.

COHEN, W. B., and SPIES, T. A., 1992, Estimating structural attributes of Douglas-fir/western hemlock forest stands from Landsat and SPOT imagery. *Remote Sensing of Environment*, **41**, 1–17.

EVERHAM, E. E., 1996, Forest damage and recovery from catastrophic wind. *The Botanical Review*, **62**, 113–185.

FERRETTI, M., 1997, Forest health assessment and monitoring—issues for consideration. *Environmental Monitoring and Assessment*, **48**, 45–72.

FISHBEIN, E., and PATTERSON, R. T., 1992, Error-weighted maximum likelihood (EWML): a new statistically based method to cluster quantitative micropaleontological data. *Journal of Paleontology*, **67**, 475–486.

FRANKLIN, S. E., 2000, *Remote Sensing for Sustainable Forest Management*, 1st edn (New York: Lewis).

GILLIS, M. D., and LECKIE, D. G., 1993, Forest inventory mapping procedures across Canada. Canadian Forest Service Information Report PI–X–114, 79p.

GONG, P., PU, R., and MILLER, J. R., 1995, Coniferous forest LAI estimation along the Oregon transect using compact airborne spectrographic imager data. *Photogrammetric Engineering and Remote Sensing*, **61**, 1107–1117.

HADDOW, K. A., KING, D. J., POULIOT, D. A., PITT, D. G., and BELL, F. W., 2000, Early regeneration conifer identification and competition cover assessment using airborne digital frame camera imagery. *The Forestry Chronicle,* Special Issue on Remote Sensing, **76**, 11–24.

HAIR, J. F., ANDERSON, R. E., TATHAM, R. L., and BLACK, W. C., 1998, *Multivariate Data Analysis*, 4th edn (Upper Saddle River, NJ: Prentice Hall).

HALL, F. G., PEDDLE, D. R., and LEDREW, E. F., 1996, Remote sensing of biophysical variables in boreal forest stands of *Picea mariana*. *International Journal of Remote Sensing*, **17**, 3077–3081.

HARALICK, R., 1979, Statistical and structural approaches to texture. *Proceedings of the IEEE*, **67**, 786–804.

JAKUBAUSKAS, M. E., 1996, Canonical correlation analysis of coniferous forest spectral and biotic relations. *International Journal of Remote Sensing*, **17**, 2323–2332.

KAISER, H. F., 1960, The application of electronic computers to factor analysis. *Educational and Psychological Measurement*, **20**, 141–151.

KING, D. J., 1995, Airborne multispectral digital camera and video systems: a critical review of system design and applications. *Canadian Journal of Remote Sensing*, **21**, 245–273.

KING, D. J., 2000, Airborne remote sensing in forestry: sensors, analysis and applications. *The Forestry Chronicle,* Special Issue on Remote Sensing, **76**, 25–42.

KING, D. J., 2002, Forest structure, health and regeneration assessment using airborne digital camera imagery. *Proceedings of the ForestSAT Symposium, Edinburgh, UK, 5–9 August 2002* (Edinburgh: UK Forestry Commission, Forest Research), CD–ROM publication, 10p.

LAWRENCE, R. L., and RIPPLE, W. J., 1998, Comparisons among vegetation indices and bandwise regression in a highly disturbed, heterogeneous landscape: Mount St Helens, Washington. *Remote Sensing of Environment*, **64**, 91–102.

LÉVESQUE, J., and KING, D. J., 1999, Airborne digital camera image semivariance for evaluation of forest structural damage at a mine site. *Remote Sensing of Environment*, **68**, 112–124.

LÉVESQUE, J., and KING, D. J., 2003, Spatial analysis of radiometric fractions from high-resolution multispectral imagery for modelling forest structure and health. *Remote Sensing of Environment*, **84**, 589–602.

LI-COR, INC., 1991, *LAI–2000 Plant Canopy Analyzer Operating Manual* (Lincoln, NE: Li–Cor, Inc.).

OLTHOF, I., and KING, D. J., 1997, Evaluation of textural information in airborne CIR digital camera imagery for estimation of forest stand leaf area index. *Proceedings of the First North American Symposium on Small Format Aerial Photography*, *Cloquet, MN, 14–17 October 1997* (Bethesda, MD: American Society for Photogrammetry and Remote Sensing), pp.154–164.

OLTHOF, I., and KING, D. J., 2000, Development of a forest health index using multispectral airborne digital camera imagery. *Canadian Journal of Remote Sensing*, **26**, 166–175.

PCI INC., 1994, *Using PCI software, (PCI 6.2), APC algorithm* (Ontario: PCI Inc.).

PEDDLE, D. R., HALL, F. G., and LEDREW, E. F., 1999, Spectral mixture analysis and geometric optical reflectance modeling of boreal forest biophysical structure. *Remote Sensing of Environment*, **67**, 288–297.

PELLIKKA, P., SEED, E. D., and KING, D. J., 2000, Modelling deciduous ice storm damage using aerial CIR imagery and hemispheric photography. *Canadian Journal of Remote Sensing*, **26**, 394–405.

SEED, E. D., and KING, D. J., 1997, Determination of mixed boreal forest stand biophysical structure using large scale airborne digital camera imagery. *Proceedings of GER 1997/ 19th Symposium on Remote Sensing*, *Ottawa, ON, 26–29 May 1997* (Ottawa: Canadian Remote Sensing Society), CD–ROM publication. Paper #75, 8pp.

SEED, E. D., and KING, D. J., 2003, Shadow brightness and shadow fraction relations with effective LAI: importance of canopy closure and view angle in mixedwood boreal forest. *Canadian Journal of Remote Sensing,* Special Issue on Measurement and Use of Leaf Area Index in Monitoring Vegetated Ecosystems, **29**, 324–335.

ST. ONGE, B. A., and CAVAYAS, F., 1995, Estimating forest stand structure from high-resolution imagery using the directional variogram. *International Journal of Remote Sensing*, **16**, 1999–2021.

ST. ONGE, B. A., and CAVAYAS, F., 1997, Automated forest structure mapping from high-resolution imagery based on directional semivariogram estimates. *Remote Sensing of Environment*, **61**, 82–95.

STEVENS, J. M., 1996, *Applied Multivariate Statistics for the Social Sciences*, 3rd edn (Mahbah, NJ: Lawrence Erlbraum Associates).

TABACHNICK, B. G., and FIDELL, L. S., 1996, *Using Multivariate Statistics,* 3rd edn (New York: Harper Collins College Publishers).

WALSWORTH, N. A., and KING, D. J., 1999, Image modelling of forest changes associated with acid mine drainage. *Computers and Geosciences*, **25**, 567–580.

WULDER, M. A., LAVIGNE, M. B., LEDREW, E. F., and FRANKLIN, S. E., 1997, Comparison of texture algorithms in the statistical estimation of LAI: first-order, second-order, and semivariance moment texture (SMT). *Proceedings of GER 1997/19th Symposium on Remote Sensing, Ottawa, ON, 24–30 May 1997* (Ottawa: Canadian Remote Sensing Society), CD–ROM publication, Paper #160, 10pp.

WULDER, M. A., LEDREW, E. F., FRANKLIN, S. E., and LAVIGNE, M. B., 1998, Aerial image texture information in the estimation of northern deciduous and mixed wood forest leaf area index (LAI). *Remote Sensing of Environment*, **64**, 64–76.

YUAN, X., KING, D. J., and VLCEK, J., 1991, Sugar maple decline assessment based on spectral and textural analysis of multispectral aerial videography. *Remote Sensing of Environment*, **37**, 47–54.